Phytochemistry 194 (2022) 113025

Contents lists available at ScienceDirect

Phytochemistry

journal homepage: www.elsevier.com/locate/phytochem

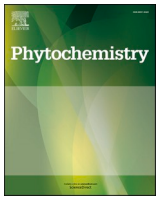

# Changes in glycosyl inositol phosphoceramides during the cell cycle of the red alga *Galdieria sulphuraria*

Milada Vítová [a], Mária Čížková [a], Vít Náhlík [a,b], Tomáš Řezanka [c,*]

[a] Institute of Microbiology of the Czech Academy of Sciences, Centre Algatech, Laboratory of Cell Cycles of Algae, Novohradská 237, 379 81 Třeboň, Czech Republic
[b] Faculty of Science, University of South Bohemia, Branišovská 1760, 370 05 České Budějovice, Czech Republic
[c] Institute of Microbiology of the Czech Academy of Sciences, Vídeňská 1083, 142 20 Prague, Czech Republic

ARTICLE INFO

*Keywords:*
*Galdieria sulphuraria*
Galdieriaceae
Red alga
Glycosyl inositol phosphoceramides
Cell cycle
Liquid chromatography-electrospray mass spectrometry

ABSTRACT

Sphingolipids are significant component of plant-cell plasma membranes, as well as algal membranes, and mediate various biological processes. One of these processes is the change in lipid content during the cell cycle. This change is key to understanding cell viability and proliferation. There are relatively few papers describing highly glycosylated glycosyl inositol phosphorylceramide (GIPC) due to problems associated with the extractability of GIPCs and their analysis, especially in algae.

After alkaline hydrolysis of total lipids from the red alga *Galdieria sulphuraria*, GIPCs were measured by high-resolution tandem mass spectrometry and fragmentation of precursor ions in an Orbitrap mass spectrometer in order to elucidate the structures of molecular species. Fragmentation experiments such as tandem mass spectrometry in the negative ion mode were performed to determine both the ceramide group and polar head structures. Measurement of mass spectra in the negative regime was possible because the phosphate group stabilizes negative molecular ions $[M\text{-}H]^-$.

*Analysis:* of GIPCs at various stages of the cell cycle provided information on their abundance. It was found that, depending on the phases of the cell cycle, in particular during division, the uptake of all three components of GIPC, i.e., long-chain amino alcohols, fatty acids, and polar heads, changes. Structural modifications of the polar headgroup significantly increased the number of molecular species. Analysis demonstrated a convex characteristic for molecular species with only one saccharide (hexose or hexuronic acid) as the polar head. For two carbohydrates, the course of Hex-HexA was linear, while for HexA-HexA it was concave. The same was true for GIPC with three and four monosaccharides.

## 1. Introduction

In eukaryotic organisms, especially in plants, sphingolipids are among the main structural lipids of cell membranes (Gronnier et al., 2016). Together with sterols and glycerolipids, sphingolipids are essential for cell membrane formation, stability, and fluidity (Blaas and Humpf, 2013; Breslow and Weissman, 2010). They also serve as signaling molecules and components of lipid rafts (Breslow and Weissman, 2010; Cacas et al., 2013; Rennie et al., 2014). The key structures of sphingolipids are long-chain bases (LCB) and fatty acids (FA). These are bound to a serine backbone, forming the basic structure of ceramide (Breslow and Weissman, 2010). Glycosyl inositol phosphoceramides (GIPCs) represent the most abundant class of sphingolipids in higher plants, comprising up to tens of percent of the plasma membrane, and have the general structure glucose (glucosamine)-glucuronic acid-inositol phosphoceramides, see Fig. 1 (Cacas et al., 2013; Markham et al., 2006; Rennie et al., 2014).

The method of choice for sphingolipid analysis is liquid chromatography connected with electrospray ionization - tandem mass spectrometry (LC-ESI-MS/MS), which provides the required structural sensitivity, specificity and relatively high throughput. Another advantage is the possibility to analyze a relatively small amount of biomass, e.g., Tellier et al. (2014) published an analysis of GIPC obtained from 2 mg of biomass. To simplify the analysis of GIPC, it is possible to perform mild alkaline hydrolysis by treatment with methylamine in the crude extract, hydrolyzing ester bonds in order to eliminate ester-containing contaminating lipids such as triacylglycerols, glycolipids, and glycerophospholipids (Bure et al., 2014; Markham et al., 2006). This treatment

* Corresponding author.
*E-mail address:* rezanka@biomed.cas.cz (T. Řezanka).

https://doi.org/10.1016/j.phytochem.2021.113025
Received 23 September 2021; Received in revised form 15 November 2021; Accepted 18 November 2021

does not affect the amide bonds of sphingolipids (Markham et al., 2006).

Identification and characterization of GIPC in plants is currently a subject of interest for lipid research (Bure et al., 2011; Cacas et al., 2013). Nevertheless, there is little information available on the presence of GIPC in algae. Two papers (Bure et al., 2014; Cacas et al., 2013) have been published in which GIPCs were identified in the algae *Chondracanthus acicularis* (formerly *Ceramium aciculare*), *Ulva lactuca*, and *Fucus vesiculosus,* representatives of marine red, green, and brown macroalgae, respectively, and also referred to as seaweed. Furthermore, unicellular green algae of the genera *Chlorella*, *Chlamydomonas*, and *Coccomyxa* were analyzed in the thesis (Rose, 2015), which, at least to the best of our knowledge, has not been further published. HPLC-ESI-MS found that hexuronic acid is not present in the genus *Chlorella,* and the majority of GIPCs comprise hexosyl-hexosyl-inositol phosphoceramide (Hex-Hex-IPC).

Processes controlling the cell cycle in eukaryotic microorganisms have been studied and characterized thoroughly over the last half-century (Fujiwara et al., 2020; Jong et al., 2021; Patterson et al., 2021; Sato et al., 2021; Zachleder et al., 2019, 2021). Successful completion of the cell cycle presents several structural challenges. Plasma and organelle membranes must expand during the cell cycle and undergo topological remodeling while maintaining their biochemical and barrier functions. The correct composition of the daughter cell membranes and their spatial arrangements must be secured. Finally, the lipid membranes must be divided to form two or more viable daughter cells. Disruption of membrane functions, improperly timed membrane lysis, or improper spatial distribution of cellular components all pose dangerous threats to cell survival that must be avoided to maintain cell viability.

The success of the cell cycle across innumerable species suggests that factors that influence the behavior, shape, and size of the membrane are carefully controlled through repeated cycles of cell division, as reported in bacteria (Furse et al., 2017), yeast (Blank et al., 2020), or green algae (Li et al., 2016; Umen, 2018). As already described for prokaryotes (Furse et al., 2017), but also the eukaryotic green alga *Desmodesmus quadricauda* (Vítová et al., 2021), the change in lipid composition was consistent with the fact that it had a significant effect on the geometry of the structures formed (Koynova and Caffrey, 1998; Mulet et al., 2008). This suggests therefore that lipids play an essential role in determining membrane behavior and thus, cell structure. Furthermore, published data (Vítová et al., 2021) show that the composition of lipid membranes is redesigned to minimize the cost of free energy when changing their shape during the cell cycle (Furse and Shearman, 2018).

The above facts lead to the hypothesis that the biosynthesis of structural lipids is associated with the cell cycle. We used synchronous cultures of the red alga *Galdieria sulphuraria* (Galdieri) Merola (Galdieriaceae) (Náhlík et al., 2021) to test this hypothesis. As an extremophile, *G. sulphuraria* is characterized by unique features developed during adaptation to its harsh environment. These features are often metabolically conditioned, which is also true for the metabolism of lipids (Vítová et al., 2016).

This study describes the optimization of extraction, mild alkaline hydrolysis, shotgun lipidomics of total GIPCs, and hydrophilic interaction liquid chromatography with mass spectrometry (HILIC/ESI-MS/MS) for analysis of a wide range of GIPC homologs differing both in the ceramide part and in the structure of the polar headgroup. In addition, the abundance of individual molecular species of GIPC was further studied during the cell cycle of the red alga *G. sulphuraria*.

## 2. Results and discussions

### 2.1. Extraction procedure, mild hydrolysis, and use of shotgun MS for GIPC identification

Extraction of GIPC from cells is usually a problem, mainly because GIPC is sparingly soluble in conventional solvent mixtures used for lipid extraction. A published article (Markham et al., 2006) compares a few methods, i.e., Bligh and Dyer (1959) (extraction by methanol:chloroform:water), Nichols (1963), and Christie and Han (2010) (chloroform:propan-2-ol), Hanson and Lester (1980) (ethanol:water:diethylether:pyridine:ammonia) and Toledo et al. (1995) (lower phase of propan-2-ol:hexane:water). The results favor method four or five. Based on these published data, the last method, i.e., extraction with a 2-propanol:n-hexane:water mixture (55:20:25, v/v/v), was the optimized GIPC extraction solvent system used.

Shotgun analysis of an algal extract harvested at zero hour was used to determine if the alga produced GIPC at all. For preliminary identification by negative ESI, the ion $[C_3PO_3–C_1–CO_2]^-$ at *m/z* 373.0540

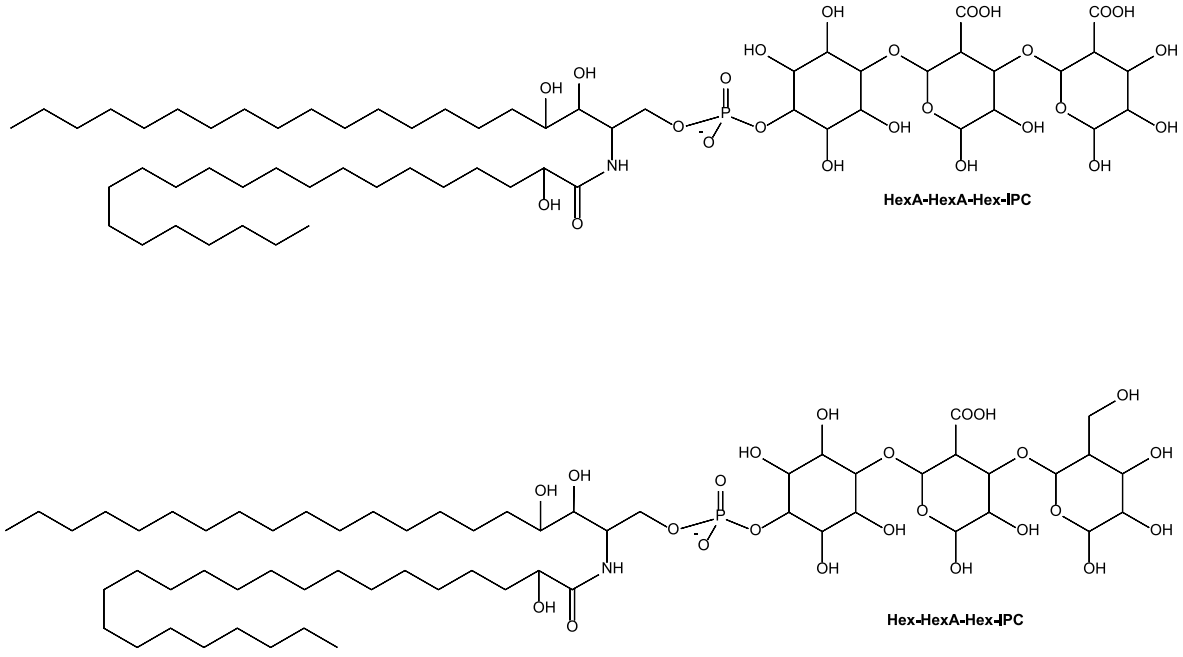


**Fig. 1.** Glycosyl inositol phosphoceramides (GIPC) have the general structure glucose (glucosamine)-glucuronic acid-inositol phosphoceramides.

($C_{11}H_{18}O_{12}P^-$) was selected (Fig. 1S). Bure et al. (2011) described its presence in all GIPC (from series A to series F). The *m/z* value is not affected by changes in the hydrocarbon chains, i.e., fatty acids or long-chain bases. The ion structure contains hexuronic acid (without COOH) and inositol phosphate. Therefore, it is an ideal ion describing the polar head of GIPC, i.e., it is a marker for GIPC. Panzenboeck et al. (2020) indicated a value of 373.057 Da for the ion $[C_3PO_3–C_1–CO_2]^-$. This value is very similar to the value represented in this paper, differing by only 3 ppm. The presence of this ion confirmed that the red alga *G. sulphuraria* produces GIPC; see text below.

Fig. 2 shows the precursor ion scan (PIS) at *m/z* 373.0540 of the crude extract of the red alga *G. sulphuraria,* harvested at zero hour. The mass differences in the negatively charged molecular ions $[M-H]^-$ were Δ ~14 Da and its multiples, indicating different chain lengths with one, two, or more additional methylene groups. Gradual extension by methylene group(s) indicates an odd and even carbon chain number of the sphingoid base or fatty acid. Based on this analysis, see Table 1S for dozens of molecular species assumed, we confirmed that *G. sulphuraria* produces several classes of GIPC, i.e. Hex-IPC, HexA-IPC, Hex-HexA-IPC, HexA-HexA-IPC, Hex-Hex-HexA-IPC, and Hex-Hex-Hex-HexA-IPC. In addition, there are several dozen homologs of different lengths of hydrocarbon chains in each class. In total, almost 100 molecular species have been preliminarily identified by negative ESI. Further analyses were performed to elucidate the structures of these molecular species and especially changes in their abundance during various stages of the cell cycle.

Sphingolipids, including GIPC, are generally stable to hydrolysis by weak bases. Since the extraction of commonly occurring phospholipids would still be incomplete using a 2-propanol:n-hexane:water mixture, the total crude extract was subjected to mild alkaline hydrolysis using monomethylamine (Bure et al., 2014; Markham and Jaworski, 2007; Markham et al., 2006). Monomethylamine is a volatile and mild base capable of hydrolyzing lipids containing esters (e.g., phospholipids or triacylglycerols) but not sphingolipids. Fig. 3 shows the HILIC separation of the *G. sulphuraria* extract and standards. After mild hydrolysis, in addition to sphingolipids (six classes; numbers **27**–**32**, see Fig. 3), only sterols (numbers **5** and **6**) and free fatty acids (No. **7**), including one unidentified class (peak **23**), were present. Unfortunately, peak **23** could not be identified. Based on tandem MS, we believe it is also a mixture of sphingolipid homologs (different long chains bases and fatty acids) but with an unknown polar head structure. The main homolog at *m/z* 1436.7239 $[C_{62}H_{121}NO_{29}P_3]^-$ was cleaved in tandem MS and two highly abundant ions, i.e., ion at *m/z* 743.0608 $[C_{18}H_{34}O_{25}P_3]^-$ (polar head) and the ion at *m/z* 710.6666 $[C_{44}H_{88}NO_5]^-$, i.e., probably ceramide containing 2-hydroxylignoceric acid and phytosphingosine (2-amino--octadecane-1,3,4-triol), were obtained.

Tandem mass spectra were monitored in the negative ion mode for all $[M-H]^-$ ions, and their fragmentations were compared with the data of Blaas and Humpf (2013). Fragment ions in the tandem mass spectra were labeled according to GIPC nomenclature see.Tables 2S and 3S The group of polar heads in Fig. 2S consists of hexose-hexuronic acid inositol phosphate or hexuronic acid-hexuronic acid inositol phosphate (Fig. 3S). The differences manifested themselves both in the terminal saccharide part (COOH versus $CH_2OH$ groups) and in the ceramides (different chain lengths of hydroxy fatty acids). The tandem mass spectra were made possible because the mass spectrometer Orbitrap was operated in high-resolution mode. Resolution 110,000 was sufficient to distinguish between ions 1276.7184 Da and 1276.7554 Da (Δm = 0.037 Da). A resolution value of about 34,400 would be sufficient. The collision-induced dissociation (CID) tandem mass spectra of the ions at *m/z* 1276.7184 and *m/z* 1276.7554 are shown in Figs. 4 and 5. They have a similar fragmentation, differing by ~14 Da only in the saccharide part. Some ions arising from the ceramide part of the molecule differed by the same value due to different lengths of hydrocarbon chains of hydroxy fatty acids. All ion values, including abundances and the probable structure of these ions, are given in Tables 2S and 3S

Additional hexoses and/or pentoses in the polar head of the GIPC have been identified in many organisms (Bure et al., 2014; Cacas et al., 2013) therefore, tandem MS higher homologs of GIPC were screened for those mass differences. Based on both shotgun analysis and the

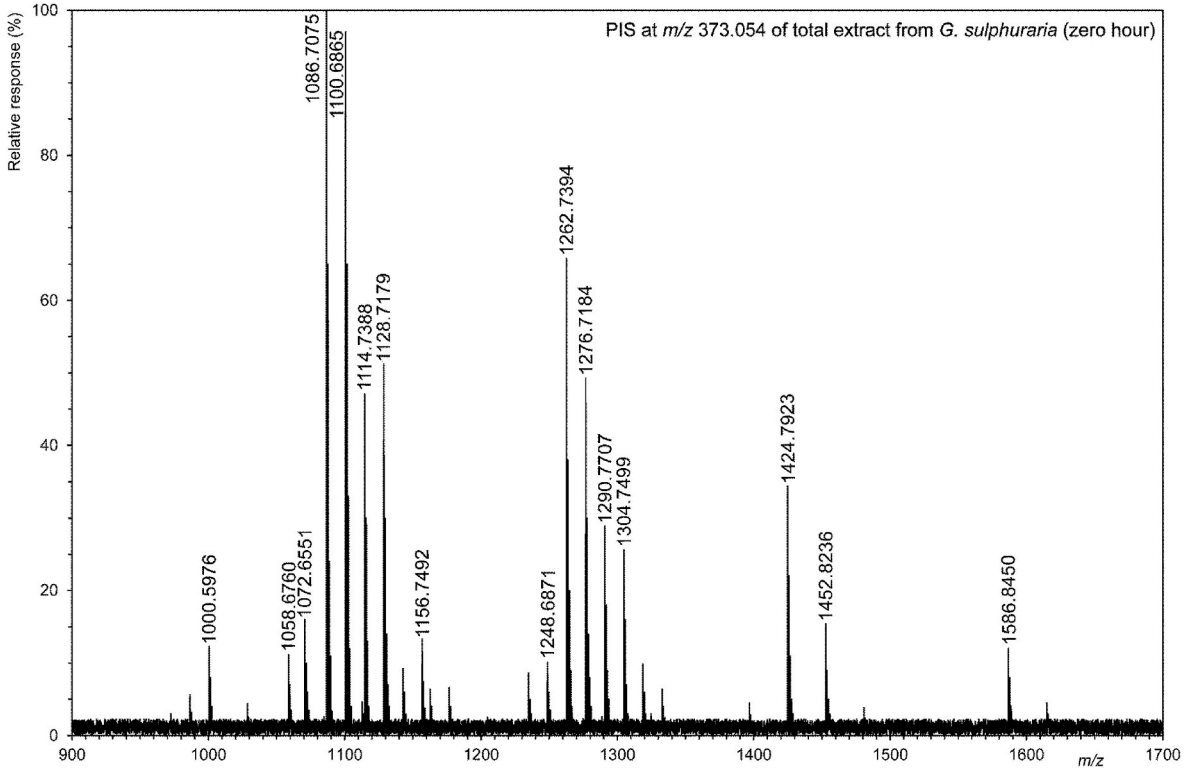


**Fig. 2.** Shotgun of precursor ion scan (PIS) at *m/z* 373.0540 of total extract from *G. sulphuraria* (zero hour).

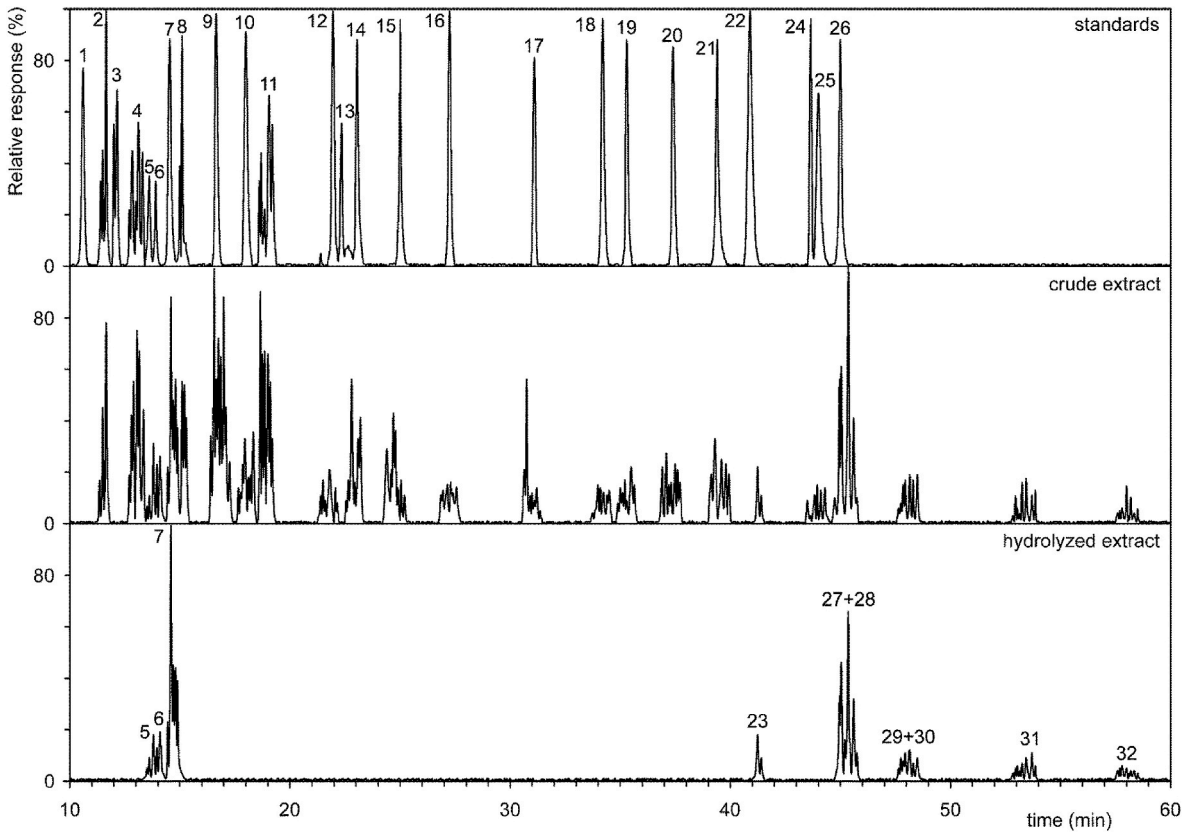


**Fig. 3.** HILIC separation of standards and the *G. sulphuraria* extract.

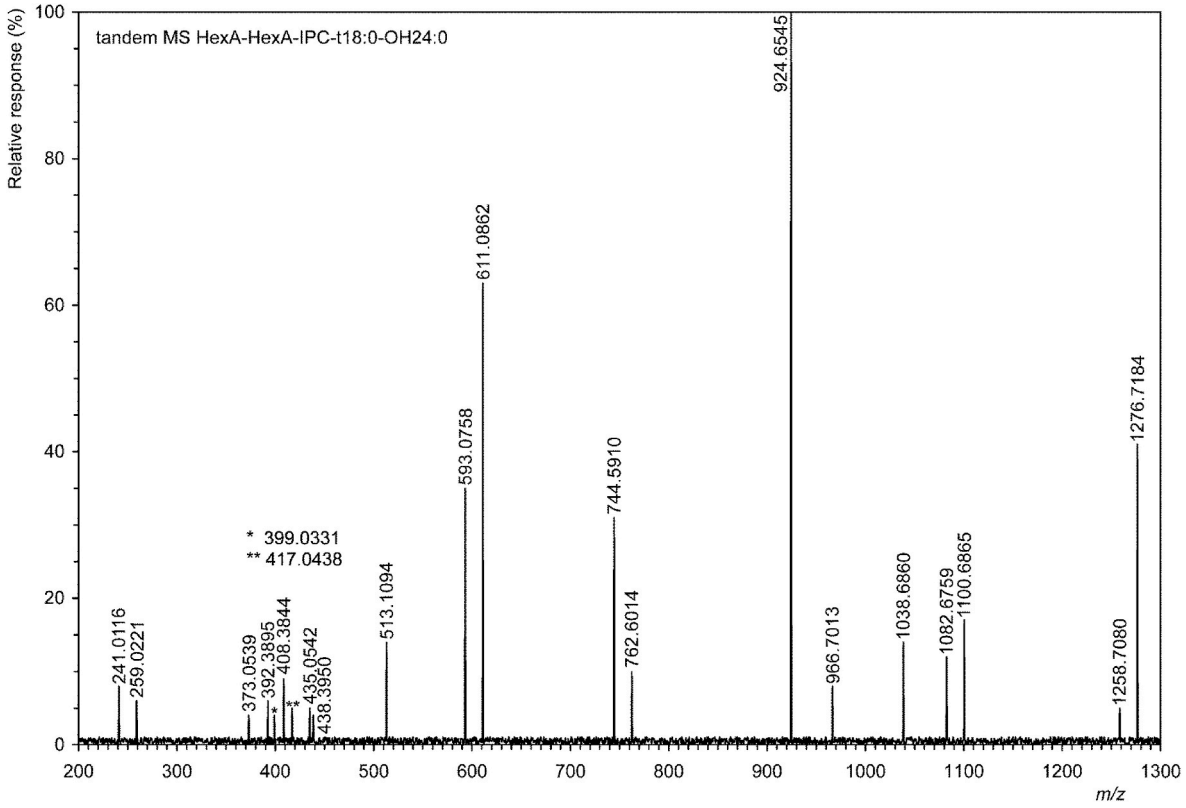


**Fig. 4.** The collision-induced dissociation (CID) tandem mass spectra of ions at *m/z* 1276.7184.

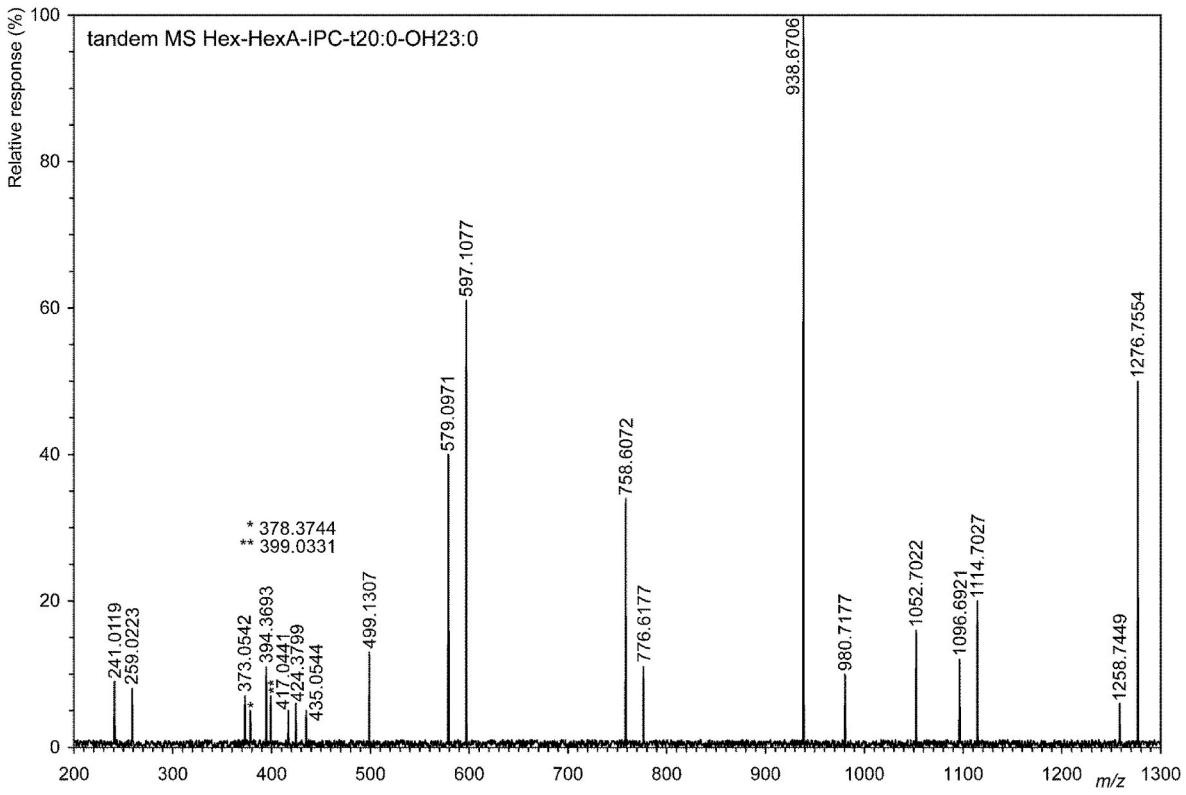


**Fig. 5.** The collision-induced dissociation (CID) tandem mass spectra of ions at *m/z* 1276.7554.

separation of total GIPC by HILIC, it was found that GIPC containing HexA-IPC with two or three other hexoses, respectively, were present. Furthermore, the peaks from HILIC were manually collected and analyzed by direct inlet in high-resolution negative ESI. The molecular species Hex-Hex-Hex-HexA-IPC-t18:0/OH24:0 was selected as an example for analysis by tandem MS. In particular, ions of the FA, S, and T type differ in the $CH_2$ group (~14.016 Da) due to the presence of 2-hydroxytetracosanoic acid instead of 2-hydroxytricosanoic acid. Fig. 4S shows the structure of the most abundant ions obtained by tandem MS of $[M\text{-}H]^-$ at 1586.8455 Da. Ions of type $[Z_0PO_3\text{–}H]^-$ at *m/z* 744.5914 ($C_{42}H_{83}NO_7P^-$) and $[Y_1\text{–}H]^-$ at *m/z* 924.6548 ($C_{48}H_{95}NO_{13}P^-$) confirm the structure of the ceramide part of the molecule, while ions $[B_3PO_3\text{–}H]^-$ at *m/z* 903.2025 ($C_{30}H_{48}O_{29}P^-$) and $[C_3PO_3\text{–}H]^-$ at *m/z* 921.2131 ($C_{30}H_{50}O_{30}P^-$) confirm the structure of the polar head. Differences between $[Y_4\text{–}H]^-$, $[Y_3\text{–}H]^-$, and $[Y_3\text{–}H]^-$, $[Y_2\text{–}H]^-$ with 162.0530 Da and 162.0532 Da, respectively, correlated with the loss of two hexoses (calculated exact mass 162.0529 Da). The difference between ions of $[Y_2\text{–}H]^-$ and $[Y_1\text{–}H]^-$ correlated with 176.0319 Da, i.e., the loss of hexuronic acid (calculated exact mass 176.0321 Da), and the difference between $[Y_1\text{–}H]^-$ and $[Y_0PO_3\text{–}H]^-$ with a calculated mass of 162.0527 Da was due to the cleavage of an inositol (calculated exact mass 162.0528 Da). All the data mentioned above confirm the structures of the polar head.

These fragmentation experiments confirmed the occurrence of GIPC species having a polar head $(Hex)_3$-HexA-IPC. Furthermore, GIPCs with four sugars were identified in the seagrass (*Zostera noltii*) (Bure et al., 2014), and their presence in other plant samples was confirmed by mass spectrometric analysis (Cacas et al., 2013). Therefore, it can be assumed that GIPCs with longer oligosaccharide chains are ubiquitous in plants (Gronnier et al., 2016).

The major molecular species or ceramide structures in all GIPC classes were combinations of saturated 2-hydroxy fatty acids, whether even or odd, and phytosphingosine and its dihomo derivative, i.e., a long-chain amino-triol containing a hydrocarbon chain with 20 carbons. Three non-hydroxy fatty acids have been identified, namely palmitic, stearic, and lignoceric acids.

GIPCs in algae differ from those in mosses, gymnosperms, and monocotyledons, while dicotyledons have the most significant complexity. Algae contain inositol phosphoceramides bound to either hexuronic acid or hexose. Conversely, higher plants, i.e., monocotyledonous and dicotyledonous plants, contain more complex lipids with hexose or pentose units bound to hexouronic acid. GIPC is usually grouped into six series, as described by Buré et al. in Table 1 (Bure et al., 2011). Table 4S shows the published structures of all GIPCs found in algae. It is clear from the table that diversity in the content of the ceramide part is relatively small. Hydroxy-fatty acids, both saturated and monoenoic, with a chain length of C24 to C28, are always present, with the exception of *U. lactuca*, where hydroxy-palmitic acid is also present. Phytosphingosine and/or dehydrophytosphingosine (4-hydroxy-8--sphingenine) were always present as the major long-chain amino alcohols. Diversity in the polar head was already much more significant, e.g., in the green algae of the genus *Chlorella,* hexuronic acid was identified.

In contrast, in green algae *Coccomyxa* and *Chlamydomonas,* hexuronic acid was not identified. The red alga *Chondracanthus acicularis* also does not contain hexuronic acid, whereas, in seaweed (*Fucus vesiculosus*, class Phaeophyceae), it was present. Li et al. (2017) published a comprehensive study of sphingolipids in 17 strains of microalgae, i.e., diatoms, dinoflagellates, and haptophytes. Ceramides, mono-, di-, and trisaccharides of ceramides, but not GIPC, were identified. Nevertheless, it is clear from all the above papers that microalgae can biosynthesize sphingolipids. The above analyzes show that, firstly, it is necessary to expand the number of algae analyzed and, secondly, to unify the methodology of GIPC analysis.

Further confirmation of the possibility of biosynthesizing GIPC was obtained from GenBank, where key enzymes necessary for GIPC biosynthesis were identified in the published genome of the red alga *Galdieria sulphuraria*, i.e., inositolphosphorylceramide synthase-like protein (GenBank XP_005703814.1) and glucuronyl/*N*-

acetylglucosaminyl transferase EXT1 (Genbank XP_005708838.1). Multiple sequence alignments (MSA) of inositol phosphorylceramide synthase-like protein of different red algae *Galdieria sulphuraria* (strain 074W), *Cyanidioschyzon merolae*, *Porphyridium purpureum*, *Gracilariopsis chorda* was carried out (Fig. 5S). Furthermore, for the glucuronyl/N-acetylglucosaminyl transferase EXT1 protein of the red alga *Galdieria sulphuraria* (strain 074W) and the diatom *Fistulifera solaris,* a sequence alignment was performed (Fig. 6S), showing the conserved domains of enzymes through various algal species.

### 2.2. Change of GIPC during the cell cycle

Samples of algae taken at different stages of the cell cycle (from zero to the eighteenth hour, see Table 5S) were analyzed in the same way. Fig. 6 shows three chromatograms of GIPC at the zero, twelfth and eighteenth hours, accompanied by photomicrographs of the *G. sulphuraria* at these stages of the cell cycle. The cells started to divide into two at the twelfth hour, and four at the eighteenth hour.

Fig. 7 shows that the two aminoalcohols had completely different distributions during the cell cycle. While t18:0 had a convex course, t20:0 was concave. The only OH-FA, i.e., OH-24:0 as the major hydroxy-acid, had a concave course (Fig. 7), while all others, even non-hydroxy fatty acids, had a convex course (see also Table 6S). In the case of intact molecular species of GIPC, the situation is further complicated by the polar head, as shown in Fig. 8 and Table 6S.

The heat map in Fig. 8 shows that the GIPC abundance related to polar head structures has a concave or convex course. The abundance is convex for molecular species having only one saccharide (hexose or hexuronic acid) as the polar head. For two saccharides, the course of Hex-HexA is linear, while for HexA-HexA it is concave. The same is true for GIPC with three and four monosaccharides, respectively. In individual molecular species, the two tendencies, i.e., convexity and concavity, intersect. An example is one of the major molecular species, HexA-IPC-t18:0/OH24:0, where the abundance at the end of the cell cycle is slightly higher than at the beginning (zero versus the eighteenth hour). A completely different situation is the molecular species Hex-Hex-HexA-IPC-t18:0/OH24:0, where the abundance increases approximately halfway through the cycle and then at the 18th h is lower than at 0 h.

Similar trends were found for phospholipids in the green alga *D. quadricauda,* where the concave course of PE and PG abundance through the cell cycle was demonstrated, with PE being lower at the end of the cell cycle than at the beginning (Vítová et al., 2021). On the other hand, the course of PC abundance was convex through the cell cycle, as for GIPC, with one saccharide polar head in *G. sulphuraria*. The changes in individual lipid abundance through the cell cycle were closely correlated with their roles in membrane structure, fluidity, and remodeling (Vítová et al., 2021).

Because GIPCs have large polar heads and very-long-chain FA, they tend to aggregate with phospholipids or even with phospholipids and sterols. GIPC thus increases the membrane thickness by several nm, i.e., up to 6–7 nm, probably due to the high negativity of GIPC caused by its phosphate group and the carboxyl group from HexA in the polar head (Mamode Cassim et al., 2021). Alterations in ceramide length and hydroxylation of GIPC can alter membrane organization as well as sphingomyelin in animal cells. Plant GIPC is structurally homologous to animal gangliosides, which are absent from plants. Gangliosides are acidic glycolipids containing sialic acid in their polar head and play an important role in immunity and signal transduction in the plasma membrane. Polyglycosylated GIPC may have a similar role as gangliosides.

Our experiment showed that glycosylation of GIPC is necessary for membrane development and function. Sphingolipids promote membrane organization and rigidity, although it is unclear how sugar residues contribute to this process (Moore et al., 2021). We hypothesize that particular GIPC may promote membrane organization and stability during rapid growth. Functional differences in the stereochemistry of glycolipid carbohydrates and their effect on membrane dynamics have not been studied in detail. It has been reported that small changes in carbohydrate stereochemistry can lead to significant changes (Fogarty et al., 2020). Molecules having differences in carbohydrate stereochemistry can drastically affect membrane shape and bending (Bhattacharya et al., 2019), but the physical principles that cause these differences have not yet been elucidated.

Unfortunately, GIPCs cannot be easily extracted by conventional

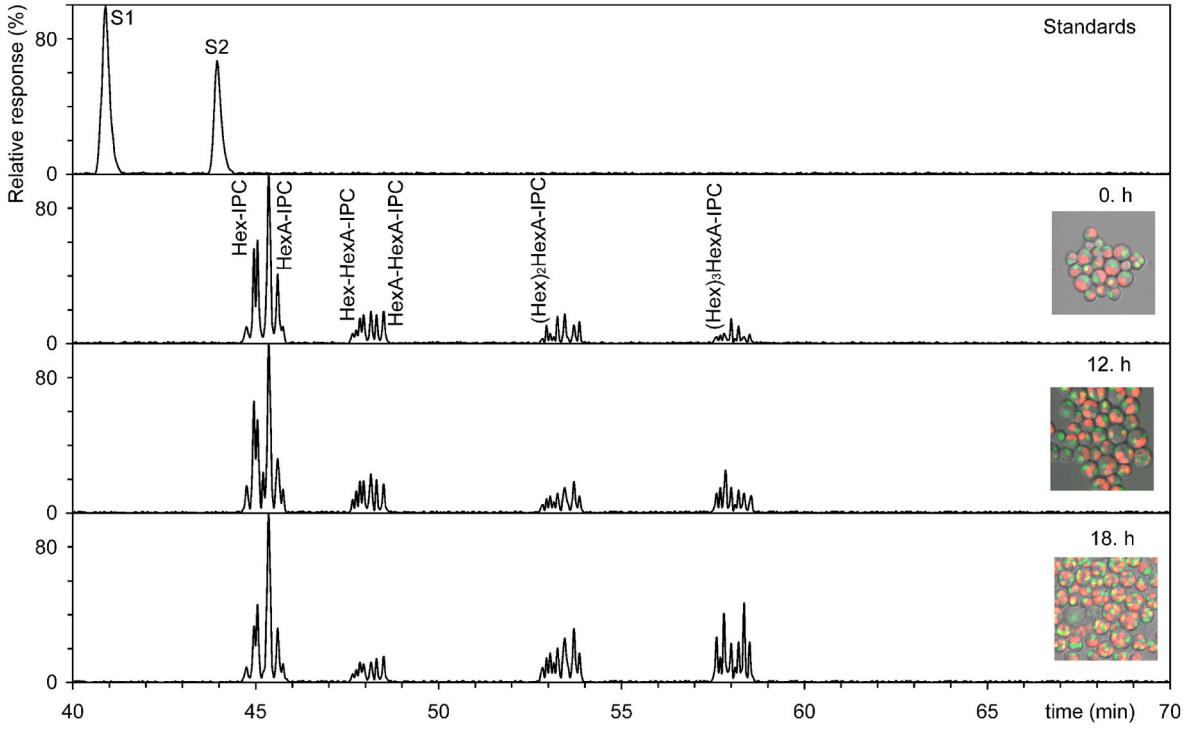


**Fig. 6.** Three chromatograms of GIPC at zero, twelfth and eighteenth hours accompanied by photomicrographs of *G. sulphuraria* at these phases of the cell cycle.

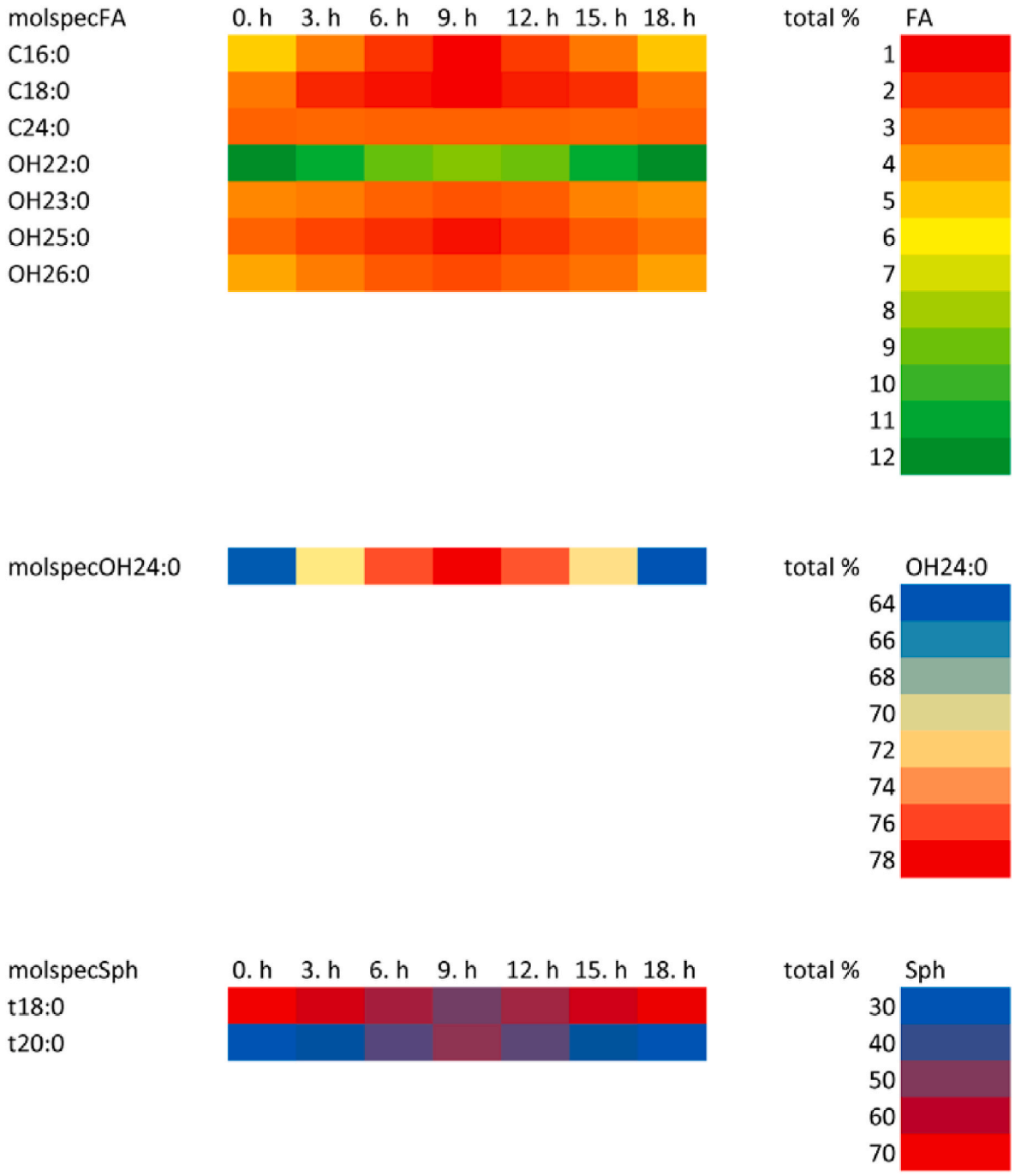


**Fig. 7.** Heat maps of aminoalcohols and hydroxy and/or non-hydroxy fatty acids during the cell cycle.

methodologies, and analysis is technically difficult, so it is often overlooked. Only with the use of the modern methods of mass spectrometry was progress made in their investigation. The consequence of these analyses is that plant membrane glycerophospholipids may be relatively less abundant than previously thought. Cacas et al. (2016) showed that GIPC is the major lipid of the tobacco (*Nicotiana tabacum*) highly-purified plasma membrane and can reach up to 40 mol% of total lipids. In *Arabidopsis thaliana* leaves, GIPC is estimated to make up 50% of plasma membrane lipids (Liu et al., 2020).

## 3. Conclusion

Structural information on GIPC sphingolipids and their polar heads in algae are rare and yet remain virtually uncharacterized. With advances in analytical chemistry, more specifically in the field of mass spectrometry, our analysis of algal GIPC represents an attempt to characterize both the static presentation and especially the differences in abundance during the cell cycle of the red alga *G. sulphuraria*.

Glycerophospholipids were removed by alkaline hydrolysis, and tandem mass spectra with high resolution and fragmentation of precursor ions in the Orbitrap mass spectrometer were measured to elucidate the molecular structures of GIPC. Fragmentation experiments such as $FTMS^2$ in the negative ion mode were performed to determine the structures of both the ceramide moiety and the structures of the polar heads. Measurements of mass spectra in the negative mode were possible because the phosphate group stabilizes negative molecular ions $[M\text{-}H]^-$. Single-charged GIPC was screened in the mass range of $m/z$ 200 to 2000 in the negative ion mode.

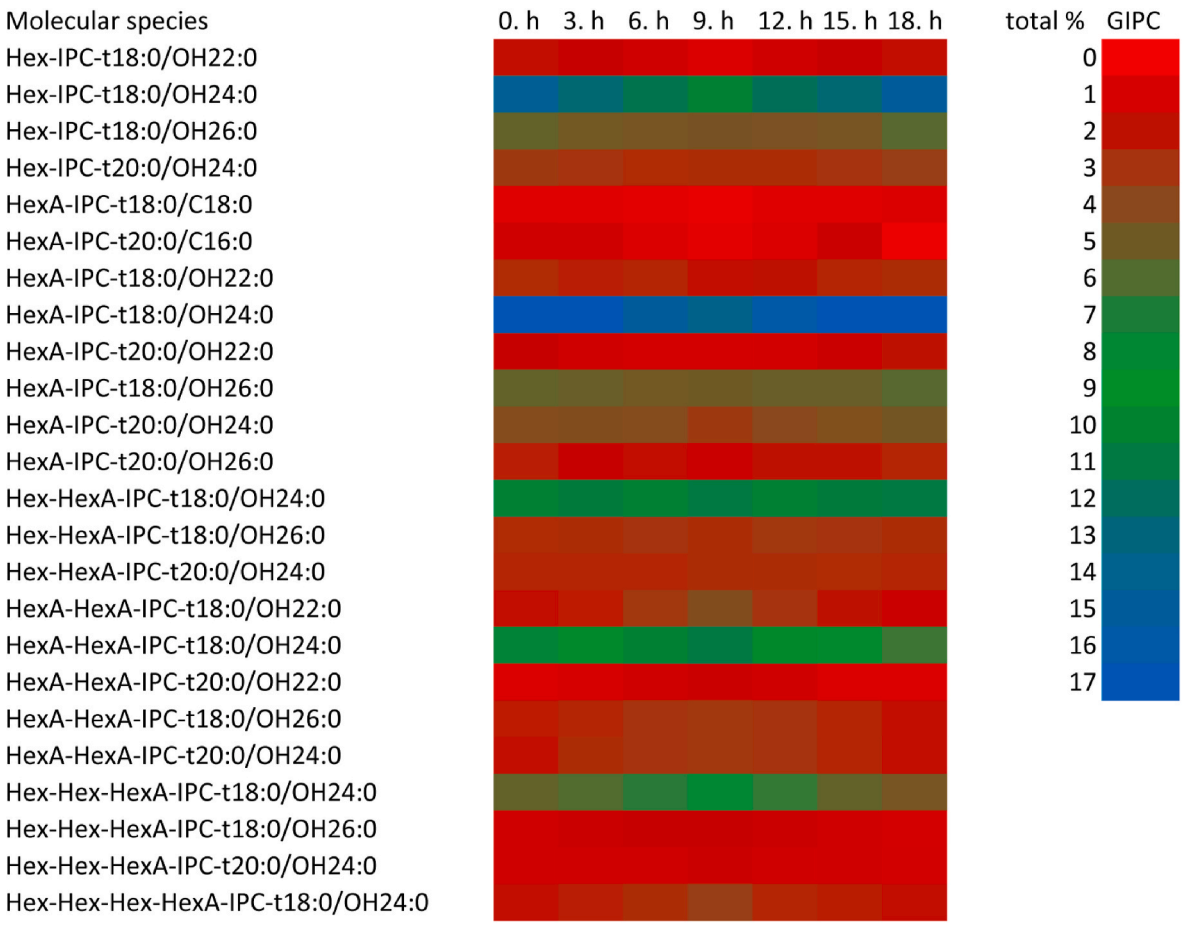


**Fig. 8.** Heat maps of intact molecular species of GIPC during the cell cycle.

GIPC analysis at various stages of the cell cycle provided results on their abundance. It was found that, depending on the stages of the cell cycle, namely during division, there was a change in the entrapment of all three components of GIPC, i.e., long-chain amino alcohols, fatty acids, and polar heads. The structural modifications of polar heads significantly increased the number of molecular species. Further research should focus on the pattern of GIPC glycosylation. This paper thus opens the way to address the function of plant glycosylated sphingolipids in the organization and function of membranes.

## 4. Experimental

### 4.1. Standards

D-glucosyl-ß-1,1′-*N*-oleoyl-D-erythro-sphingosine (S1), D-lactosyl-ß-1,1′-*N*-oleyol-D-erythro-sphingosine (S2), and sphingosyl phosphoinositol (D-erythro-sphingosyl phosphoinositol) were purchased from Sigma (Prague, Czech Republic), SYBR Green I from ThermoFisher Scientific (Linz, Austria). All other reagents used were of analytical grade and purchased from Merck (Prague, Czech Republic) or Penta (Chrudim, Czech Republic).

### 4.2. Algal cell cultures and growth conditions

The unicellular red alga *Galdieria sulphuraria* (Galdieri) Merola (Galdieriaceae) 002 was obtained from the Algal Collection of Dipartimento delle Scienze Biologiche, Section of Plant Biology, University "Federico II" of Naples, Italy.

Cells of *G. sulphuraria* from a 3-week-old agar plate were used to inoculate the batch culture to be synchronized. The synchronization itself was carried out by alternating light/dark periods, the lengths chosen according to the growth parameters of the cells (Náhlík et al., 2021). For the cell cycle experiment, a synchronized culture was diluted at the beginning of the light period to the initial DM of 100 μg $mL^{-1}$. The light/dark (L/D) cycle at the optimal conditions was set as 16/8 h L/D. Sampling was conducted every hour to evaluate the cell cycle parameters. The sampling for the GIPC analyses was done every 3 h. For cultivation details see Supplements.

### 4.3. Confocal microscopy

To follow the cell cycle progress, confocal microscopy was employed. The algal cells were stained with SYBR Green (see Supplements). The cells were observed under an LSM Zeiss 880 confocal microscope (Carl Zeiss, Jena, Germany) using the following excitation wavelengths: chlorophyll - 633 nm, and SYBR Green I - 405 nm.

### 4.4. Preparation of lipid extracts and mild alkaline hydrolysis

Total sphingolipids were extracted according to (Markham and Jaworski, (2007)) with some modifications. Briefly, lyophilized algal biomass (zero to 18th hour) was homogenized in 5 mL of isopropanol. After adding 0.5 ml of hexane and 1 ml of water, the homogenate was incubated at 60 °C for 10 min. After centrifugation, the insoluble residue was extracted twice more with an isopropanol/hexane/water bottom phase (55:25:20, *v/v/v*). The combined extracts were evaporated to dryness. GIPC was hydrolyzed by treatment with methylamine, according to (Markham et al., (2006)). Briefly, mild alkaline hydrolysis was performed with methylamine for 60 min at 50 °C. The solution was evaporated and the residue was dissolved in

tetrahydrofuran/methanol/water (2:1:2, *v/v/v*, containing 0.1% formic acid) and analyzed by mass spectrometry.

### 4.5. Shotgun lipidomics

An LTQ-Orbitrap Velos mass spectrometer (Thermo Fisher Scientific, San Jose, CA, USA), a high-resolution hybrid mass spectrometer equipped with a heated electrospray interface (H-ESI), was operated in negative ionization mode. Flow Injection Analysis (FIA) was used for sample introduction into the H-ESI ion source. Methanol:acetonitrile: aqueous 1 mM ammonium acetate (10:70:20, *v/v/v*) was used at a flow rate of 150 μL/min. The MS scan range was performed in the Fourier transform mode and recorded within a window between 200 and 2000 *m/z*. The ion spray voltage was set at −2.5 kV in the negative ionization mode with the following parameters: sheath gas flow, 18 arbitrary units (AU); auxiliary gas flow, 7 AU; ion source temperature, 250 °C; capillary temperature, 230 °C; capillary voltage, 50 V; and tube lens voltage, 170 V. Helium was used as a collision gas for collision-induced dissociation (CID) experiments. The CID normalization energy of 35% was used for the fragmentation of parental ions. The MS/MS product ions were detected in high-resolution FT mode. The calibration of the MS spectrometer was conducted using a Pierce LTQ Orbitrap negative ion calibration solution (Thermo Fisher Scientific, San Jose, CA, USA). The internal lock mass was used in the acquisition of mass spectra, i.e., 255.2330 Da, $[M-H]^-$ of palmitic acid in negative ESI. The mass accuracy was better than 0.9 ppm. The chemical structures of compounds were confirmed with the help of the spectral database LIPID MAPS® Lipidomics Gateway (http://www.lipidmaps.org/).

### 4.6. HILIC-MS-ESI

The HPLC equipment consisted of a 1090 Win system, PV5 ternary pump and automatic injector (HP 1090 series, Hewlett Packard, USA), and two Ascentis® Express HILIC connected in series, 2.7 μm particle size, L × I.D. 150 mm × 4.6 mm Merck (formerly Supelco, Prague, Czech Republic) with an injection volume of 30 μL. HPLC was performed at a flow rate of 0.95 mL/min with a linear gradient from the mobile phase containing methanol: acetonitrile:aqueous 1 mM ammonium acetate (50:30:20, *v/v/v*) to methanol:acetonitrile:aqueous 1 mM ammonium acetate (10:70:20, *v/v/v*) for 60 min. The column temperature was 35 °C and the re-equilibration period between runs was 30 min. The 10% HPLC flow was introduced into the ESI source, and 90% of the flow containing fractions of lipid classes was collected manually. In order to have sufficient material, the fractionation was repeated up to five times, and the corresponding fractions were pooled, evaporated to dryness, and re-dissolved in an appropriate volume of the mobile phase. The system backpressure reached 1000 bars during gradient analysis. The LTQ Orbitrap Velos (Thermo Fisher Scientific, Bremen, Germany) high-resolution hybrid mass spectrometer was used for the ESI-MS analysis under the conditions described above.

## Declaration of competing interest

The authors declare that they have no known competing financial interests or personal relationships that could have appeared to influence the work reported in this paper.

## Acknowledgments

This research was funded by the European fund for regional development, the program Interreg V-A Austria – Czech Republic, grant number ATCZ172 REEgain, and with institutional support RVO 61388971 and the COST Action 19116 – PLANTMETALS. We acknowledge Mgr. Adéla Vaňková for confocal imaging and prof. J. D. Brooker for critical reading and language editing of the text.

## Appendix A. Supplementary data

Supplementary data to this article can be found online at https://doi.org/10.1016/j.phytochem.2021.113025.

## References

Bhattacharya, A., Brea, R.J., Song, J.J., Bhattacharya, R., Sinha, S.K., Devaraj, N.K., 2019. Single-chain beta-D-glycopyranosylamides of unsaturated fatty acids: self-assembly properties and applications to artificial cell development. J. Phys. Chem. B 123, 3711–3720. https://doi.org/10.1021/acs.jpcb.9b01055.

Blaas, N., Humpf, H.U., 2013. Structural profiling and quantitation of glycosyl inositol phosphoceramides in plants with Fourier transform mass spectrometry. J. Agric. Food Chem. 61, 4257–4269. https://doi.org/10.1021/jf4001499.

Blank, H.M., Papoulas, O., Maitra, N., Garge, R., Kennedy, B.K., Schilling, B., Marcotte, E. M., Polymenis, M., 2020. Abundances of transcripts, proteins, and metabolites in the cell cycle of budding yeast reveal coordinate control of lipid metabolism. Mol. Biol. Cell 31, 1069–1084. https://doi.org/10.1091/mbc.E19-12-0708.

Bligh, E.G., Dyer, W.J., 1959. A rapid method of total lipid extraction and purification. Can. J. Biochem. Physiol. 37, 911–917. https://doi.org/10.1139/o59-099.

Breslow, D.K., Weissman, J.S., 2010. Membranes in balance: mechanisms of sphingolipid homeostasis. Mol. Cell. 40, 267–279. https://doi.org/10.1016/j.molcel.2010.10.005.

Bure, C., Cacas, J.L., Wang, F., Gaudin, K., Domergue, F., Mongrand, S., Schmitter, J.M., 2011. Fast screening of highly glycosylated plant sphingolipids by tandem mass spectrometry. Rapid Commun. Mass Spectrom. 25, 3131–3145. https://doi.org/10.1002/rcm.5206.

Bure, C., Cacas, J.L., Mongrand, S., Schmitter, J.M., 2014. Characterization of glycosyl inositol phosphoryl ceramides from plants and fungi by mass spectrometry. Anal. Bioanal. Chem. 406, 995–1010. https://doi.org/10.1007/s00216-013-7130-8.

Cacas, J.L., Bure, C., Furt, F., Maalouf, J.P., Badoc, A., Cluzet, S., Schmitter, J.M., Antajan, E., Mongrand, S., 2013. Biochemical survey of the polar head of plant glycosylinositolphosphoceramides unravels broad diversity. Phytochemistry 96, 191–200. https://doi.org/10.1016/j.phytochem.2013.08.002.

Cacas, J.L., Bure, C., Grosjean, K., Gerbeau-Pissot, P., Lherminier, J., Rombouts, Y., Maes, E., Bossard, C., Gronnier, J., Furt, F., Fouillen, L., Germain, V., Bayer, E., Cluzet, S., Robert, F., Schmitter, J.M., Deleu, M., Lins, L., Simon-Plas, F., Mongrand, S., 2016. Revisiting plant plasma membrane lipids in tobacco: a focus on sphingolipids. Plant Physiol. 170, 367–384. https://doi.org/10.1104/pp.15.00564.

Christie, W.W., Han, X., 2010. Lipid Analysis - Isolation, Separation, Identification and Lipidomic Analysis. Oily Press, Woodhead Publishing. https://doi.org/10.1533/9780857097866.

Fogarty, C.A., Harbison, A.M., Dugdale, A.R., Fadda, E., 2020. How and why plants and human N-glycans are different: insight from molecular dynamics into the "glycoblocks" architecture of complex carbohydrates. Beilstein J. Org. Chem. 16, 2046–2056. https://doi.org/10.3762/bjoc.16.171.

Fujiwara, T., Hirooka, S., Ohbayashi, R., Onuma, R., Miyagishima, S.Y., 2020. Relationship between cell cycle and diel transcriptomic changes in metabolism in a unicellular red alga. Plant Physiol. 183, 1484–1501. https://doi.org/10.1104/pp.20.00469.

Furse, S., Shearman, G.C., 2018. Do lipids shape the eukaryotic cell cycle? Biochim. Biophys. Acta (BBA)-Mol. Cell Biol. Lipids 1863, 9–19. https://doi.org/10.1016/j.bbalip.2017.09.010.

Furse, S., Jakubec, M., Rise, F., Williams, H.E., Rees, C.E., Halskau, Ø., 2017. Evidence that *Listeria innocua* modulates its membrane's stored curvature elastic stress, but not fluidity, through the cell cycle. Sci. Rep. 7, 1–11. https://doi.org/10.1038/s41598-017-06855-z.

Gronnier, J., Germain, V., Gouguet, P., Cacas, J.L., Mongrand, S., 2016. GIPC: glycosyl inositol phospho ceramides, the major sphingolipids on earth. Plant Signal. Behav. 11, e1152438 https://doi.org/10.1080/15592324.2016.1152438.

Hanson, B.A., Lester, R.L., 1980. The extraction of inositol-containing phospholipids and phosphatidylcholine from *Saccharomyces cerevisiae* and *Neurospora crassa*. J. Lipid Res. 21, 309–315. https://doi.org/10.1016/S0022-2275(20)39810-2.

Jong, L.W., Fujiwara, T., Hirooka, S., Miyagishima, S.Y., 2021. Cell size for commitment to cell division and number of successive cell divisions in cyanidialean red algae. Protoplasma 258, 1103–1118. https://doi.org/10.1007/s00709-021-01628-y.

Koynova, R., Caffrey, M., 1998. Phases and phase transitions of the phosphatidylcholines. Biochim. Biophys. Acta Rev. Biomembr. 1376, 91–145. https://doi.org/10.1016/S0304-4157(98)00006-9.

Li, Y., Liu, D., Lopez-Paz, C., Olson, B.J., Umen, J.G., 2016. A new class of cyclin dependent kinase in *Chlamydomonas* is required for coupling cell size to cell division. Elife 5, e10767. https://doi.org/10.7554/eLife.10767.

Li, Y.R., Lou, Y.M., Mu, T., Ke, A.Y., Ran, Z.S., Xu, J.L., Chen, J.J., Zhou, C.X., Yan, X.J., Xu, Q.S., Tan, Y.H., 2017. Sphingolipids in marine microalgae: development and application of a mass spectrometric method for global structural characterization of ceramides and glycosphingolipids in three major phyla. Anal. Chim. Acta 986, 82–94. https://doi.org/10.1016/j.aca.2017.07.039.

Liu, N.J., Wang, N., Bao, J.J., Zhu, H.X., Wang, L.J., Chen, X.Y., 2020. Lipidomic analysis reveals the importance of GIPCs in *Arabidopsis* leaf extracellular vesicles. Mol. Plant 13, 1523–1532. https://doi.org/10.1016/j.molp.2020.07.016.

Mamode Cassim, A., Navon, Y., Gao, Y., Decossas, M., Fouillen, L., Grelard, A., Nagano, M., Lambert, O., Bahammou, D., Van Delft, P., Maneta-Peyret, L., Simon-Plas, F., Heux, L., Jean, B., Fragneto, G., Mortimer, J.C., Deleu, M., Lins, L., Mongrand, S., 2021. Biophysical analysis of the plant-specific GIPC sphingolipids

reveals multiple modes of membrane regulation. J. Biol. Chem. 296, 100602. https://doi.org/10.1016/j.jbc.2021.100602.

Markham, J.E., Jaworski, J.G., 2007. Rapid measurement of sphingolipids from *Arabidopsis thaliana* by reversed-phase high-performance liquid chromatography coupled to electrospray ionization tandem mass spectrometry. Rapid Commun. Mass Spectrom. 21, 1304–1314. https://doi.org/10.1002/rcm.2962.

Markham, J.E., Li, J., Cahoon, E.B., Jaworski, J.G., 2006. Separation and identification of major plant sphingolipid classes from leaves. J. Biol. Chem. 281, 22684–22694. https://doi.org/10.1074/jbc.M604050200.

Moore, W.M., Chan, C., Ishikawa, T., Rennie, E.A., Wipf, H.M.L., Benites, V., Kawai-Yamada, M., Mortimer, J.C., Scheller, H.V., 2021. Reprogramming sphingolipid glycosylation is required for endosymbiont persistence in *Medicago truncatula*. Curr. Biol. 31, 2374–2385. https://doi.org/10.1016/j.cub.2021.03.067.

Mulet, X., Templer, R.H., Woscholski, R., Ces, O., 2008. Evidence that phosphatidylinositol promotes curved membrane interfaces. Langmuir 24, 8443–8447. https://doi.org/10.1021/la801114n.

Náhlík, V., Zachleder, V., Čížková, M., Bišová, K., Singh, A., Mezricky, D., Řezanka, T., Vítová, M., 2021. Growth under different trophic regimes and synchronization of the red microalga *Galdieria sulphuraria*. Biomolecules 11, 939. https://doi.org/10.3390/biom11070939.

Nichols, B.W., 1963. Separation of lipids of photosynthetic tissues - improvements in analysis by thin-layer chromatography. Biochim. Biophys. Acta 70, 417–422. https://doi.org/10.1016/0926-6542(63)90060-X.

Panzenboeck, L., Troppmair, N., Schlachter, S., Koellensperger, G., Hartler, J., Rampler, E., 2020. Chasing the major sphingolipids on earth: automated annotation of plant glycosyl inositol phosphoceramides by glycolipidomics. Metabolites 10, 375. https://doi.org/10.3390/metabo10090375.

Patterson, J.O., Basu, S., Rees, P., Nurse, P., 2021. CDK control pathways integrate cell size and ploidy information to control cell division. Elife 10, e64592. https://doi.org/10.7554/eLife.64592.

Rennie, E.A., Ebert, B., Miles, G.P., Cahoon, R.E., Christiansen, K.M., Stonebloom, S., Khatab, H., Twell, D., Petzold, C.J., Adams, P.D., Dupree, P., Heazlewood, J.L., Cahoon, E.B., Scheller, H.V., 2014. Identification of a sphingolipid alpha-glucuronosyltransferase that is essential for pollen function in *Arabidopsis*. Plant Cell 26, 3314–3325. https://doi.org/10.1105/tpc.114.129171.

Rose, S., 2015. A Lipidomics Approach to the Viral-Host Dynamics of the Unicellular, Eukaryotic Alga *Chlorella Variabilis* and its Viral Pathogen, PBCV-1, vol. 77. Dissertations Theses Biol. Sci.. https://digitalcommons.unl.edu/dissertations/AAI3738581

Sato, M., Kakui, Y., Toya, M., 2021. Tell the difference between mitosis and meiosis: interplay between chromosomes, cytoskeleton, and cell cycle regulation. Front. Cell Develop. Biol. 9, 660322. https://doi.org/10.3389/fcell.2021.660322.

Tellier, F., Maia-Grondard, A., Schmitz-Afonso, I., Faure, J.D., 2014. Comparative plant sphingolipidomic reveals specific lipids in seeds and oil. Phytochemistry 103, 50–58. https://doi.org/10.1016/j.phytochem.2014.03.023.

Toledo, M.S., Suzuki, E., Straus, A.H., Takahashi, H.K., 1995. Glycolipids from *Paracoccidioides brasiliensis* - isolation of a galactofuranose-containing glycolipid reactive with sera of patients with paracoccidioidomycosis. J. Med. Vet. Mycol. 33, 247–251. https://doi.org/10.1080/02681219580000501.

Umen, J.G., 2018. Sizing up the cell cycle: systems and quantitative approaches in *Chlamydomonas*. Curr. Opin. Plant Biol. 46, 96–103. https://doi.org/10.1016/j.pbi.2018.08.003.

Vítová, M., Goecke, F., Sigler, K., Řezanka, T., 2016. Lipidomic analysis of the extremophilic red alga *Galdieria sulphuraria* in response to changes in pH. Algal Res.-Biomass Biofuels Bioproducts 13, 218–226. https://doi.org/10.1016/j.algal.2015.12.005.

Vítová, M., Lanta, V., Čížková, M., Jakubec, M., Rise, F., Halskau, Ø., Bišová, K., Furse, S., 2021. The biosynthesis of phospholipids is linked to the cell cycle in a model eukaryote. Biochim. Biophys. Acta (BBA)-Mol. Cell Biol. Lipids 1866, 158965. https://doi.org/10.1016/j.bbalip.2021.158965.

Zachleder, V., Ivanov, I., Vítová, M., Bišová, K., 2019. Effects of cyclin-dependent kinase activity on the coordination of growth and the cell cycle in green algae at different temperatures. J. Exp. Bot. 70, 845–858. https://doi.org/10.1093/jxb/ery391.

Zachleder, V., Ivanov, I.N., Kselíková, V., Bialevich, V., Vítová, M., Ota, S., Takeshita, T., Kawano, S., Bišová, K., 2021. Characterization of growth and cell cycle events as affected by light intensity in the green alga *Parachlorella kessleri*, as a new model for cell cycle research. Biomolecules 11, 891. https://doi.org/10.3390/biom11060891.